Downloaded form http://iranpaper.ir

International Journal of Adhesion & Adhesives 59 (2015) 27–39

Contents lists available at ScienceDirect

International Journal of Adhesion & Adhesives

journal homepage: www.elsevier.com/locate/ijadhadh

Influence of bonding technique on bond behavior of CFRP-to-clay brick masonry joints: Experimental study using particle image velocimetry (PIV)

Ardalan Hosseini*, Davood Mostofinejad, Mehran Emami

Department of Civil Engineering, Isfahan University of Technology (IUT), Isfahan 84156-83111, Iran

ARTICLE INFO

Article history:
Accepted 26 January 2015
Available online 3 February 2015

Keywords:
Unreinforced masonry (URM)
CFRP sheet
Clay brick
Single lap-shear test
Bond strength
EBROG technique
Particle Image velocimetry (PIV)

ABSTRACT

This paper presents a comparative study on the performance of three different techniques for bonding carbon fiber reinforced polymer (CFRP) sheets to masonry substrate. To do so, eight CFRP-to-clay brick masonry joints were prepared using conventional externally bonded reinforcement (EBR) technique, with and without surface preparation. Moreover, for the first time, grooving method (GM) in the form of externally bonded reinforcement on grooves (EBROG) technique was used for bonding CFRP sheets to masonry substrate in six other joints. The specimens were tested under single lap-shear loading and the influence of bonding technique as well as effect of fiber reinforced polymer (FRP) bond length were comprehensively investigated and discussed based on the experimental results. A non-contact full field deformation measurement technique, i.e. particle image velocimetry (PIV), was used to obtain the load–slip diagrams, strain profiles along the bonded length, and strain fields of all tested specimens. Experimental results and PIV measurements demonstrated that bond behavior of CFRP sheets attached to masonry substrate was significantly improved by using EBROG technique. Consequently, the technique can be used as an alternative to conventional EBR method to more efficiently utilize the tensile capacity of FRPs used for external strengthening of unreinforced masonry (URM) structures.

© 2015 Elsevier Ltd. All rights reserved.

1. Introduction

Unreinforced masonry (URM) structures, which constitute both a significant portion of the world's heritage buildings and a substantial component of the modern residential building stock, are susceptible to brittle failure when subjected to loads induced by extreme wind and earthquakes [1,2]. Consequently, strengthening of masonry construction to resist higher in-plane or out-of-plane loads is of great importance and interest worldwide. As well as in strengthening of reinforced concrete (RC) structures, fiber reinforced polymers (FRPs) have attracted lots of interest for masonry rehabilitation. This growing interest in FRP application can be attributed to the unique material characteristics including corrosion resistant, light weight, and high strength-to-weight ratio, as well as ease of application, minimal esthetic impact, and reversibility character, which are required in the strengthening of historic structures [3,4].

Despite certain advantages of composite technology, one of the main concerns about strengthening of masonry structures with FRPs, especially carbon FRPs (CFRPs), is utilization of the full tensile capacity of the composite. In other words, owing to the lower tensile strength of masonry compared to concrete, application of CFRP composites for strengthening of masonry structures is seriously questionable. The reason is that occurrence of *debonding* which is the predominant mode of failure in FRP strengthened members, leads to waste of the relatively expensive composite material [4,5].

Due to the importance of the issue, several numerical and experimental studies have been conducted to increase the existing knowledge on bond behavior of externally bonded masonry systems and to improve the bond strength of externally bonded reinforcement (EBR) FRPs to masonry substrate by using novel bonding techniques [1–14]. It is demonstrated that using near surface mounted (NSM) instead of conventional externally bonded reinforcements can significantly improve the bond behavior of FRP-to-masonry [1,2,10,11]. However, suitable FRP reinforcements in NSM technique are thin rectangular strips and bars, and not sheets and fabrics; the most efficient reinforcement cross-sectional shape to choose is a thin rectangular strip

Abbreviations: CCD, charge-coupled device; CFRP, carbon fiber reinforced polymer; EB, externally bonding; EBR, externally bonded reinforcement; EBRIG, externally bonded reinforcement in grooves; EBROG, externally bonded reinforcement on grooves; FB, fracture in brick; FRP, fiber reinforced polymer; GM, grooving method; NES, near-end supported; NSM, near surface mounted; PIV, particle image velocimetry; RC, reinforced concrete; URM, unreinforced masonry; WS, without surface preparation; WSS, wedge-shaped splitting

* Corresponding author. Tel.: +98 31 33913818; fax: +98 31 33912700.
E-mail addresses: a.hosseini@cv.iut.ac.ir, ardalanhsn@gmail.com (A. Hosseini).

http://dx.doi.org/10.1016/j.ijadhadh.2015.01.015
0143-7496/© 2015 Elsevier Ltd. All rights reserved.

Downloaded form http://iranpaper.ir

[10]. Furthermore, research studies have shown that utilizing different anchorage systems may also improve the efficiency of EBR systems [12–14]. It is important to recognize, however, all anchoring systems are highly problematic due to the brittle and anisotropic nature of masonry as well as composite materials; as a result, any proposed method of anchorage should be highly scrutinized before field implementation [15]. On the other hand, although numerous investigations on the application of anchorage systems in concrete and masonry strengthening are now available, existing information would not allow development of a design procedure, even for concrete applications [16].

In 2010, a novel bonding technique called grooving method (GM) was introduced by Mostofinejad and Mahmoudabadi [17] as an alternative to EBR for flexural strengthening of concrete beams with FRP. GM consisted of cutting grooves into tension face of concrete beams, filling the grooves with proper epoxy adhesive, and bonding FRP sheets on the member's surface over the filled grooves. The main idea of the technique was to increase the probable failure plane within the concrete, and subsequently, increase the bond strength of FRP-to-concrete. Primary results, conducted on small-scale concrete beams, demonstrated that cutting 3 longitudinal grooves having $3 \times 10\ mm^2$ (width × depth) dimensions completely eliminated debonding of 70 mm wide CFRP sheets with net thickness of fibers equal to 0.12 mm from concrete beam specimens, and increased the ultimate loads up to 80% compared with conventional EBR strengthened specimens [17].

Grooving method in its original form was later referred as externally bonded reinforcement on grooves (EBROG) technique. Performance of EBROG technique for flexural strengthening of RC beams using multilayer CFRP sheets was further investigated by Mostofinejad et al. [18] and promising results were reported in complete elimination of debonding failure mode. Recently, another technique for GM named as externally bonded reinforcement in grooves (EBRIG) was also introduced by Mostofinejad and Shameli [19] in which the FRP is formed in contact with the surfaces of the grooves using wet layup procedure. The superiority of both EBROG and EBRIG techniques over the conventional EBR method for flexural strengthening of RC beams was comprehensively discussed by Mostofinejad et al. [20].

Bond behavior of CFRP sheets attached to concrete using EBR and EBROG techniques was studied in depth through single lap-shear tests by Hosseini and Mostofinejad [21]. Experimental results showed that EBROG technique operates more effectively than EBR; premature debonding failure was completely eliminated when EBROG technique was used [21]. More recently, Hosseini and Mostofinejad [22] investigated different effects of groove characteristics on CFRP-to-concrete bond behavior of EBROG joints using a full field deformation measurement technique. Experimental results demonstrated that utilizing EBROG technique, even with small shallow grooves, significantly improves interfacial fracture characteristics (such as peak interfacial shear stress and fracture energy) of CFRP-to-concrete bonded joints [22].

The great performance of EBROG technique in strengthening of concrete members has been verified in [17–22]. Thus, for the first time, the current study presents application of the technique for strengthening of masonry structures. As a first step, the efficiency of the technique should be accurately assessed, and the results should be compared with the conventional EBR method. Consequently, a test series of 14 CFRP-to-clay brick masonry joints were prepared using the conventional EBR method (with and without surface preparation) and EBROG technique. The specimens were tested under single lap-shear loading, while an image-based full field deformation measurement technique was utilized to comprehensively investigate the influence of different bonding techniques on bond behavior of CFRP-to-clay brick masonry joints.

2. Specimen preparation and test setup

2.1. Specimens details and material properties

Single lap-shear bond tests were carried out through 14 masonry prism specimens with dimensions of $220 \times 100 \times 520\ mm^3$ (width × height × length). Each masonry prism specimen was comprised of eight 10-hole (two rows of five cores with diameter of 33 mm) fired clay brick units with nominal dimensions of $220 \times 100 \times 55\ mm^3$ (length × width × height) and 10-mm thick mortar joints. The mortar consisted of normal Portland cement and sand mixed in a cement:sand ratio of 1:3, having a water/cement ratio of 0.5 by weight. Different ancillary tests were carried out to evaluate the mechanical characteristics of the utilized brick units, mortar, and masonry prisms. The rupture modulus and compressive strength of brick units were tested on the basis of ASTM C67-05 [23] equal to 5.5 and 16.4 MPa, determined as the mean values of 5 three-point flexural tests and 5 compression tests, respectively. The 28-day compressive strength of the mortar was also determined as 22.9 MPa using 8 cubic specimens based on ASTM C190-05 [24]. Furthermore, compressive strength tests were conducted on five masonry prism specimens, each comprised of five brick units, to determine the modulus of elasticity and ultimate compressive strength of the masonry. The mean values of the elasticity modulus and compressive strength of the masonry were determined as 3998 and 22.8 MPa, respectively.

The FRP composite used in the current study was made up of unidirectional carbon fibers fabricated via wet layup process. A two-component epoxy adhesive was used for bonding FRP composite to the masonry prisms as well as for matrix phase of the FRP composite. Mechanical properties of carbon fibers and epoxy resin utilized in this study are provided in Table 1 according to the manufacturer's catalog. It should be noted that the presented value of 4300 MPa for ultimate capacity of fibers cannot be achieved in wet layup systems as previously mentioned by the authors [21]. The ultimate load capacity of the composite suggested by the manufacturer is 350 kN/m for a typical 1.0 mm thick laminate produced using the 0.131 mm thick carbon fibers impregnated with the epoxy adhesive. Consequently, the effective ultimate stress of carbon fibers can be calculated equal to 2670 MPa based on the net properties of the fibers. It is also worth mentioning that no ancillary tension test on FRP coupons was conducted as part of the current study. However, coupon tests previously conducted on the same material [21] indicated an average ultimate stress of 2795 MPa for the carbon fibers. Thus, the latter value was used in the current study as the ultimate strength of the utilized carbon fibers.

2.2. Testing layout

A total of 14 bond tests on CFRP-to-masonry were conducted in four series (i.e. series I–IV). Series I–III, each consisted of four specimens, were designed to investigate the influence of bonding technique on bond behavior of CFRP-to-masonry. The specimens

Table 1
Properties of FRP materials.

	Type	Thickness (mm)	Tensile strength (MPa)	Elastic modulus (GPa)	Elongation at break (%)
Fibers	SikaWrap 230C	0.131	4300	238	1.8
Adhesive	Sikadur 330	0.5–0.9	30	4.5	0.9

Downloaded form http://iranpaper.ir

in series I and II were strengthened by CFRP sheets using conventional EBR method; no surface preparation was used in series I, while grinding was used for surface preparation of the specimens in series II. Series III was designed to evaluate the performance of GM in the form of EBROG technique. Detailed discussions on different bonding techniques are provided in the subsequent sections. Apart from investigating the influence of bonding technique, two different FRP bond lengths (L_f=100 and 200 mm) were also considered in series I through III to examine the effect of L_f on bond behavior of CFRP-to-masonry in different bonding techniques. The notation of test specimens in series I–III is *T-m-n*, where *T* refers to bonding technique (WS=externally bonding without surface preparation; EB=externally bonding using grinding; and GM=grooving method in the form of EBROG technique); *m* identifies FRP bond length in mm (100 or 200); and *n* distinguishes the ordinal number of each test (1 or 2). Furthermore, the two specimens in series IV, designated as GM*-100-1(2), were designed to investigate the effect of groove width on the performance of EBROG technique. Note that, except the above aforementioned parameters, all other experimental parameters such as CFRP width and thickness remained constant and equal to b_f= 48 mm and t_f=0.131 mm, respectively. A detailed description of the specimens specifications is provided in Table 2.

Table 2
Specimens specifications.

Series	Specimen label	Bonding technique	b_f (mm)	L_f (mm)	b_g (mm)	d_g (mm)
I	WS-100-1	EBR (without surface preparation)	48	100	–	–
	WS-100-2		48	100	–	–
	WS-200-1		48	200	–	–
	WS-200-2		48	200	–	–
II	EB-100-1	EBR (using grinding)	48	100	–	–
	EB-100-2		48	100	–	–
	EB-200-1		48	200	–	–
	EB-200-2		48	200	–	–
III	GM-100-1	EBROG	48	100	5	10
	GM-100-2		48	100	5	10
	GM-200-1		48	200	5	10
	GM-200-2		48	200	5	10
IV	GM*-100-1	EBROG	48	100	10	10
	GM*-100-2		48	100	10	10

b_f=width of CFRP strip; L_f=CFRP bond length; b_g=groove width; d_g=groove depth.

2.3. Specimen preparation via different bonding techniques

2.3.1. Externally bonding without surface preparation

Preparing the specimens in series I via conventional EBR technique without surface preparation (hereafter referred as WS specimens) consisted of three main steps: (1) cleaning the masonry surface using compressed air; (2) repairing the probable surface unevenness and applying the resin undercoat; (3) installing the carbon fiber sheet followed by an adhesive overcoat. An image of a masonry prism just before step 2 is shown in Fig. 1a.

2.3.2. Externally bonding using grinding

Preparation of the specimens in series II (hereafter referred as EB specimens) is quite similar to that of the WS specimens; but, a light grinding was used in this series prior to bonding procedure (Fig. 1b). The preparation procedure in this series consisted of four main steps: (1) light grinding the surface using a disk grinder; (2) properly cleaning the surface using compressed air; (3) repairing the masonry surface and applying the resin undercoat; and (4) installing the carbon fiber sheet followed by an adhesive overcoat.

2.3.3. EBROG technique

To strengthen the specimens in series III via EBROG technique (hereafter referred as GM specimens), two 5×10 mm^2 (width $\times$ depth) longitudinal grooves having a center-to-center distance of 25 mm were cut into each specimen face using a circular saw (Fig. 2a). The grooves length was exactly equal to the FRP bond length of each specimen, i.e. 100 or 200 mm. It is worth mentioning that a special support was designed for the circular saw to accurately adjust the grooves depth [22]. The grooves were then cleaned with compressed air to remove dust and were fully filled with epoxy adhesive (Fig. 2b). Immediately after, carbon fiber sheets were bonded to the concrete surface over the grooves followed by an adhesive overcoat (Fig. 2c). Note that preparing the specimens in series IV was exactly the same as the above mentioned procedure; but the grooves were 10-mm wide.

2.3.4. Embedding natural colored sand

In order to obtain full field deformation measurements, it was intended to use image analysis technique. Thus, it was necessary for the captured images to have a texture to create features upon which image processing can properly operate [21,22]. Since CFRP sheet does not show a suitable texture, natural colored sand between sieve nos. 50 and 100, obtained from mixing equal proportions of five different colors was embedded to all specimens' face just after end

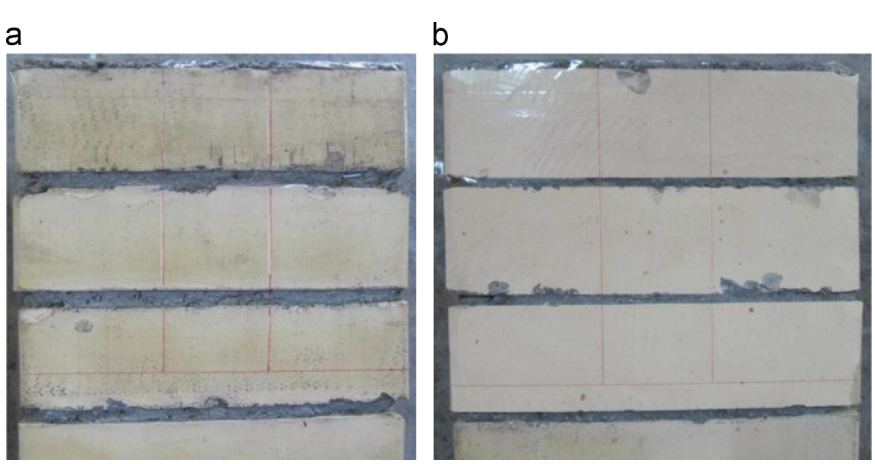

Fig. 1. Specimen preparation in series I and II. (a) Series I (without surface preparation) and (b) Series II (surface preparation using grinding).

Downloaded form http://iranpaper.ir

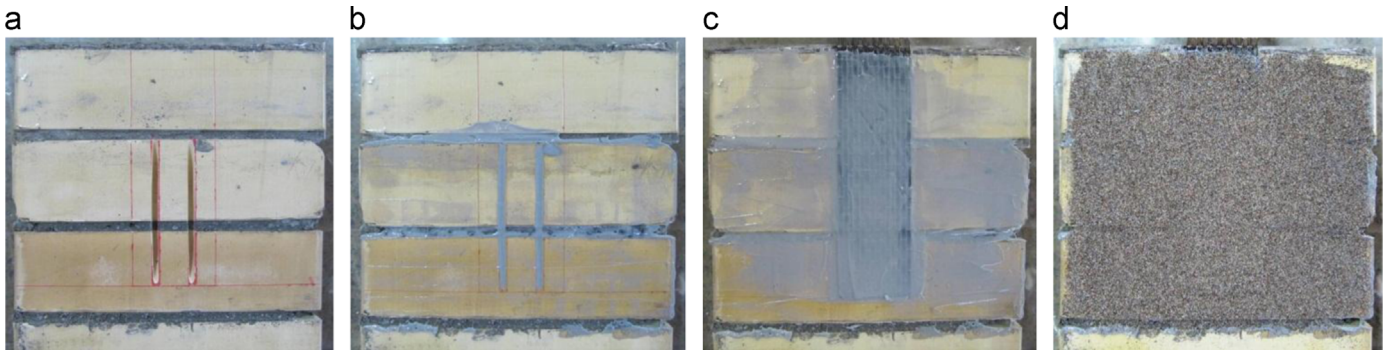

Fig. 2. Strengthening via EBROG technique. (a) Cutting two longitudinal grooves, (b) Filling the grooves using epoxy adhesive, (c) Adhering carbon fibers over the grooves and (d) Embedding natural colored sand.

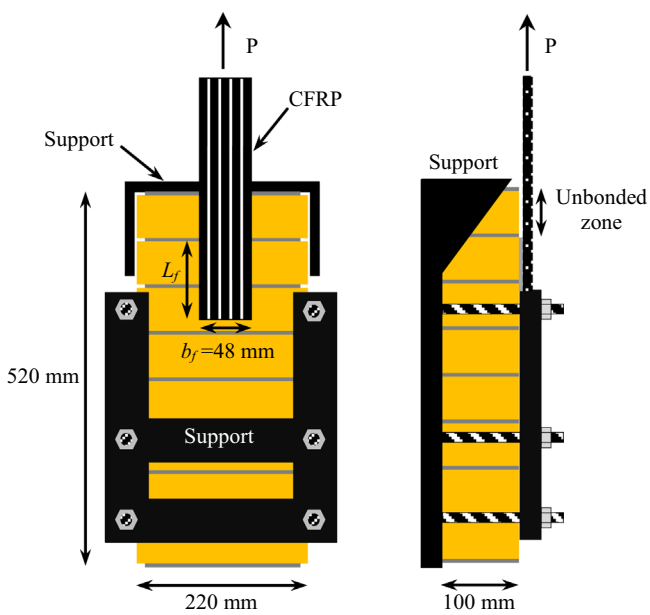

Fig. 3. Specimen dimensions and loading arrangement.

of strengthening procedure and before epoxy hardening (Fig. 2d). Obviously, embedded sand has no effect on CFRP-to-masonry bond behavior [22,25]. The specimens were cured for at least 7 days in laboratory condition before testing to ensure strength development of the epoxy resin.

2.4. Test setup

Single lap-shear loading was applied by means of a 300 kN hydraulic jack, specially designed and manufactured for bond tests in structural laboratory of Isfahan University of Technology (IUT). All tests were performed under displacement control with a speed of 2.0 mm/min. Specimen dimensions and loading arrangement are shown in Fig. 3. Since the compression reaction of support may cause stress concentration at the loaded edges of prism specimens in near-end supported (NES) single lap-shear tests [26], the first brick unit of the masonry prisms was left unbonded to eliminate any probable stress concentration (Fig. 3). Note that similar consideration for eliminating stress concentration at the loaded end of FRP composites, in NES single lap-shear tests, was taken into account by other researchers [4,27,28]. As it is illustrated in Fig. 3, a special steel frame was also designed in the current study to eliminate any probable rotation and tilting of the masonry prisms during single lap-shear loading.

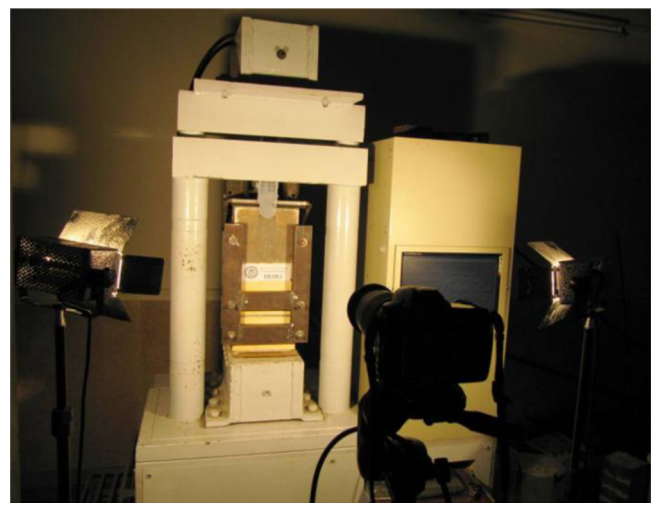

Fig. 4. Test setup.

Since it was intended to evaluate the whole deformations of the test specimens by means of digital image analysis technique, one CCD-camera (charge-coupled device), i.e. Nikon D80 with resolution of 10.0 megapixels (3872 × 2592 pixels) having a Nikkor (18–135 mm) lens was placed perpendicular to the specimens' face at a distance equal to 1.5 m. The specimens were illuminated using two white light projectors to eliminate any probable parasitic lights. Digital images were automatically captured from each specimen undergoing deformation using a remote control at regular intervals. A digital data logger was used to monitor the load cell measurements and image numbers simultaneously. Test setup including specimen arrangement, camera and projectors positions, and the testing machine is shown in Fig. 4.

3. Deformation measurements using particle image velocimetry (PIV)

An accurate image-based deformation measurement technique, called particle image velocimetry (PIV), was utilized in this study to comprehensively investigate bond behavior of CFRP-to-masonry. PIV is originally a velocity-measuring technique which was first developed by Adrian [29] in the field of experimental fluid mechanics. A modified approach was introduced by White et al. [30] to implement PIV in geotechnical testing. In the current study, the modified approach of White et al. [30] was used to obtain full field deformation measurements in each test. To do so, successive digital images captured during test process, were analyzed using GeoPIV8 software developed by White and Take [31] at Cambridge University. Since a detailed review on the PIV technique is beyond the scope of the

Downloaded form http://iranpaper.ir

current paper, readers are referred to White et al. [30] for further information on the procedure; besides, necessary discussions on the PIV technique are provided in the following sections. It should be noted that application of the PIV technique in structural tests, as well as the capability of the technique to accurately investigate the bond behavior of CFRP sheets attached to concrete substrate have been comprehensively discussed by Hosseini and Mostofinejad [21,22, 25,32]. Further consideration required for application of digital image analysis techniques in bond tests of FRP-to-concrete (masonry) is given by Carloni and Subramaniam [4,28,33].

4. Results and discussions

4.1. Failure modes

Experimental test results including failure mode, ultimate load, P_u, and increase in ultimate load over WS specimens are provided in Table 3. Typical specimens failures are also shown in Fig. 5. As it is presented in Table 3, the dominant failure mode of WS and EB specimens was debonding. It was observed that a thin layer of brick, approximately equal to 1 mm, was attached to the debonded strips (Fig. 5a and b). Hence, this failure mode is named as "fracture in brick (FB)" since the specimens failed due to masonry failure adjacent to the adhesive–masonry interface. On the other hand, specimen WS-200-2 failed through a mix-mode of failure, i.e. fracture in brick combined with debonding in brick–adhesive interface (Fig. 5a). This can be attributed to the poor bond, caused due to lack of surface preparation in this series.

As it is presented in Table 3, more complex failure modes occurred in specimens of series III and IV strengthened via EBROG technique. It was observed that the most probable failure mode in GM specimens was wedge-shaped splitting (WSS) in brick at end of the bond length combined with debonding at CFRP–adhesive interface over the grooves (DIG) (see Fig. 5). As it is illustrated in Fig. 6, the depth of the failure plane in EBR joints is approximately equal to 1 mm (Fig. 6a); while utilizing epoxy-filled grooves in EBROG technique significantly increased the depth of the failure plane within the masonry. Hence, the failure occurred due to wedge-shaped splitting in the masonry beyond the grooves depth (Fig. 6b). It is worth mentioning that the failure plane in GM specimens was approximately equal to 11 mm. In addition to WSS/DIG failure, CFRP rupture also occurred in specimens GM-100-2 and GM∗-100-2 (Fig. 5). However, it was not possible to detect the sequence of different failures due to the sudden and brittle nature of these failure modes. To the authors' opinion, the CFRP strip reached its ultimate capacity in specimens GM-100-2 and GM∗-100-2, and suddenly ruptured. Immediately after, WSS/DIG failure occurred due to the impact load created by the sudden rupture of CFRP strip. In other words, it is believed that CFRP rupture first occurred in specimens GM-100-2 and GM∗-100-2, then followed by WSS/DIG failure; because the contrariwise case seems to be impossible. Note that occurrence of the same phenomenon in CFRP-to-concrete EBROG joints was previously reported and discussed by Hosseini and Mostofinejad [22].

Apart from the above aforementioned modes of failure, mortar joint failure occurred through testing the specimens EB-100-2 and GM∗-100-1. It was not clear that when exactly the mortar joint failed during the loading process; however, after completion of the test, it was observed that the masonry prisms of the aforementioned specimens were broken from the location of one of the mortar joints (Fig. 5d). This mode of failure can be the result of poor workmanship during construction of these masonry prisms. It is believed that this phenomenon had not a significant effect on the bond behavior of CFRP-to-masonry in these specimens, because the special supports prevented any probable movements of the brick units, even in case of failure of the mortar joints. Further discussion on the issue is provided in (Section 4.5).

Table 3
Test results.

Series	Specimen label	Failure mode	P_u (kN)	$P_{u,avg}$ (kN)	α (%)	ε_f (%)	η (%)
I	WS-100-1	FB	10.33	9.93	–	0.66	57
	WS-100-2	FB	9.52				
	WS-200-1	FB	9.24	9.52	–	0.64	54
	WS-200-2	FB/DI	9.80				
II	EB-100-1	FB	8.48	9.14	−8.0	0.61	52
	EB-100-2	FB/MF	9.80				
	EB-200-1	FB	10.66	11.18	17.4	0.75	64
	EB-200-2	FB	11.69				
III	GM-100-1	WSS/DIG	14.23	14.45	45.5	0.97	82
	GM-100-2	CFRP rupture/WSS/DIG	14.66				
	GM-200-1	WSS/DIG	14.71	15.23	60.0	1.02	87
	GM-200-2	WSS/FB/DIG	15.84				
IV	GM∗-100-1	WSS/DIG/MF	13.72	14.31	44.1	0.96	81
	GM∗-100-2	CFRP rupture/WSS/DIG	14.89				

α=*Increase in Pu over WS specimen;* $\eta=\varepsilon_f/\varepsilon_{fu}$; FB=fracture in brick; DI=debonding in brick–adhesive interface; WSS=wedge-shaped splitting in brick at end of the bond length; DIG=debonding at CFRP–adhesive interface over the grooves; MF=mortar joint failure.

4.2. Ultimate loads

Ultimate experimental loads of different test series presented in Table 3, clearly show the superiority of GM over conventional EBR technique; since when EBROG technique was used, the bond strength of CFRP-to-masonry increased up to 60% over WS specimens. However, comparing the ultimate loads of EB specimens with reference WS specimens, implies that utilizing surface preparation had a slight negative influence on bond strength of the joints with L_f=100 mm; while an increase of 17.4% in ultimate strength of the joint with L_f=200 mm was observed. In general, it can be hypothesized that a light surface preparation may slightly increase the bond strength of the FRP-to-masonry joint if the process will not cause micro-fractures in the masonry substrate.

It can be concluded from the experimental results of Table 3 that increasing the bond length from 100 to 200 mm in WS specimens had no significant effect on the ultimate load carrying capacity of the joint, proving the important role of *effective bond length* in FRP-to-masonry just like in FRP-to-concrete joints. It is worth mentioning that the effective bond length, L_e, of WS and EB specimens had been calculated prior to test design as 81 mm based on Chen and Teng's model [34]. Thus, since the bond lengths in the current experimental layout (L_f=100, 200 mm) was selected larger than the predicted L_e, it was expected that increasing the bond length from 100 to 200 mm has no effect on bond strength of the joint. On the other hand, experimental results show that increasing bond length in EB specimens results in an increase of 22% in ultimate capacity of the joint. This can be justified by the role of mortar joints in specimens with L_f=200 mm, in which the mortar joints act as transverse grooves, leading to postpone debonding failure [17]. Note that during construction of the masonry prisms, the final surface of each specimen was tried to be properly leveled; however, a 1–2 mm depth notch inevitably occurred at the locations of mortar joints. The notches at the locations of mortar joints were fully filled with epoxy adhesive prior to bonding of CFRP sheets to the masonry. The above discussion (i.e. increasing the bond strength by increasing L_f) is also valid when CFRP sheets were attached to masonry using EBROG technique. However, in this case the increase in the bond strength was

Downloaded form http://iranpaper.ir

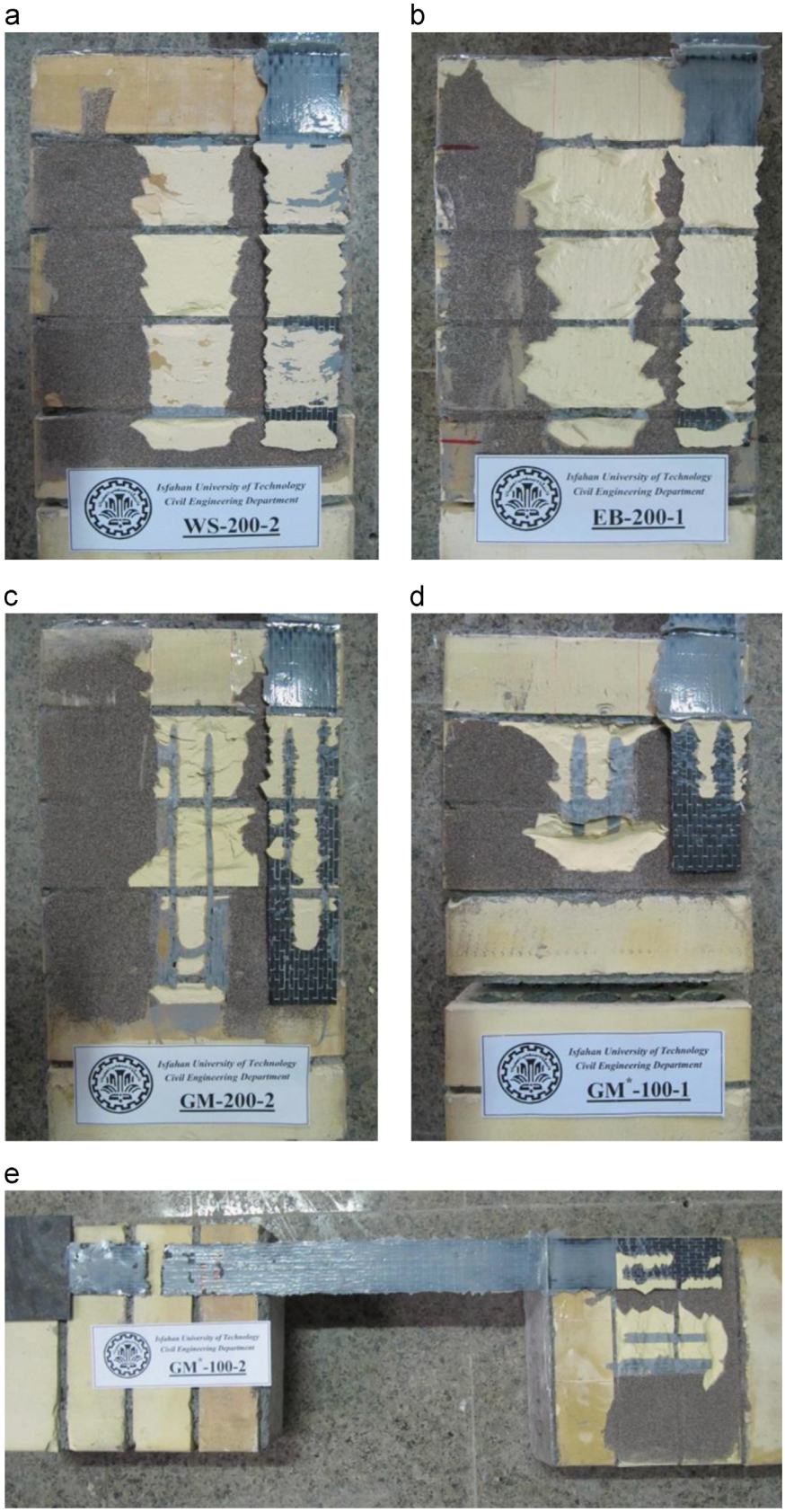

Fig. 5. Failure modes of tested specimens (FB = Fracture in brick; DI = debonding in brick–adhesive interface; WSS = wedge-shaped splitting in brick at end of the bond length; DIG = debonding at CFRP–adhesive interface over the grooves; MF = mortar joint failure). (a) WS-200-2, failure mode: FB/DI, (b) EB-200-1, failure mode: FB, (c) GM-200-2, failure mode: WSS/FB/DIG, (d) GM*-100-1, failure mode: WSS/DIG/MF and (e) GM*-100-2, failure mode: CFRP rupture/WSS/DIG.

Downloaded form http://iranpaper.ir

lower (approximately equal to 5%) compared to that of EBR technique; due to the higher influence of longitudinal grooves compared with epoxy-filled transverse notches.

It was demonstrated by Hosseini and Mostofinejad [22] that utilizing wider grooves in EBROG technique can significantly improve the interfacial characteristics of CFRP-to-concrete bonded joints, even more than deeper grooves. This was the basis of designing the series IV of specimens in the current study. However, comparing the test results of series III and IV shows that increasing the groove width had no significant effect on load carrying capacity of the masonry EBROG joints. As it was mentioned, the dominant mode of failure in masonry EBROG joints was splitting in the masonry through an approximately 11-mm deep failure plane. As a consequence, wider grooves may not change the characteristics of the failure plane. Alternatively, it is believed that deeper grooves may work more effectively in masonry EBROG joints compared to wider grooves.

FRP strain at failure, ε_f, and the efficiency factor, defined as $\eta=\varepsilon_f/\varepsilon_{fu}$, ($\varepsilon_{fu}$=ultimate FRP strain), were also calculated for each pair of identical tested specimens and are presented in Table 3. Note that the ultimate FRP strain, utilized in calculating η, was considered as $\varepsilon_{fu}=1.17\%$, based on the adopted average fibers' strength discussed in (Section 2.1). It is clear that η factor represents the percentage utilization of the tensile capacity of FRP, and hence, can be interpreted as efficiency factor of a bonding technique. It can be concluded from test results of Table 3 that the average efficiency factor of conventional EBR technique is limited to 57%, while the bond efficiency can be increased up to an average value of 83% when EBROG technique is used. Consequently, the experimental results presented in term of efficiency factor also verify the capability of GM to better utilize the tensile capacity of CFRP composites for strengthening of masonry.

4.3. Load–slip behavior

Slip of FRP reinforcement from masonry (concrete) substrate is a key factor which represents a useful reflection of FRP-to-substrate bond behavior when plotted versus load [22]. In the current study, displacements were measured through PIV analyses to calculate slip values. To do so, CFRP displacement, δ_{FRP}, as well as displacements of both upper corners of the masonry prism, $\delta_{P,L}$, and $\delta_{P,R}$, were obtained using PIV by generating 256 × 256 pixel patches (Fig. 7). Then, slip value corresponding to each digital image was calculated from the following expression [22]:

$$s=\delta_{FRP}-\frac{\delta_{P,L}+\delta_{P,R}}{2} \quad (1)$$

where s represents slip at loaded end of CFRP strip (at $x=0$); and δ_{FRP}, $\delta_{P,L}$, and $\delta_{P,R}$, are respectively CFRP displacement and deformations of masonry prism at upper corners as illustrated in Fig. 7. It is worth mentioning that the image ratio of the captured digital images was in the range of 9.46–10.15 pixel/mm. Hence, the generated 256 × 256 pixel patches had an average dimension of 26.1 mm in the object space. Consequently, the utilized patches could realistically represent the slip of the joint, considering the possible variations in deformation values of the CFRP strip along its width caused due to probable misalignments. Nevertheless, full field deformation measurements provided in Section 4.5 verify that deformation, and subsequently, strain variation along the width of the CFRP reinforcements are negligible.

Load–slip curves of tested specimens in series 2 were plotted using the aforementioned procedure, and are presented separately in Fig. 8 for L_f=100 and 200 mm. As it is illustrated in Fig. 8a, premature local debonding occurred in specimen WS-100-2 at a load of 4.5 kN, which can be attributed to poor condition of the bond. Similar local debonding also occurred in specimen EB-100-2. On the other hand, comparing the load–slip curves of specimen GM-100-2 with those of

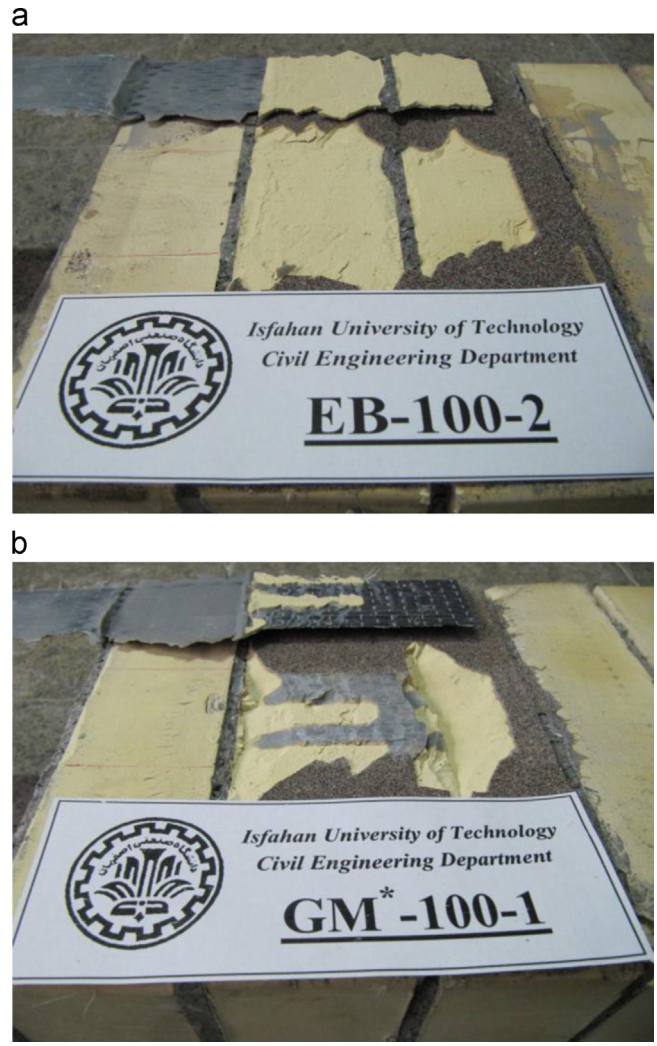

Fig. 6. Typical failure planes in masonry. (a) EBR technique and (b) EBROG technique.

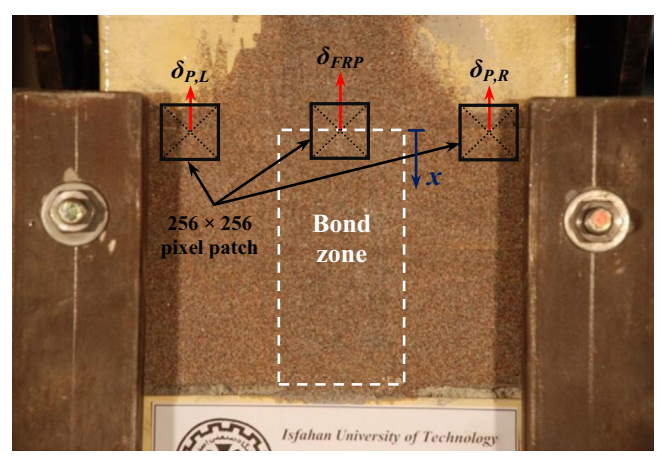

Fig. 7. Camera view and locations of different patches.

WS and EB specimens clearly verifies the superiority of EBROG technique over EBR. Since bond strength of the EBROG joint was significantly increased; while satisfying ductility, in term of ultimate slip of the joint, was also provided. As mentioned before, utilizing wider grooves in series IV of the specimens, i.e. in GM*-100-1(2), seems not to improve the ultimate load carrying capacity of the joint;

Downloaded form http://iranpaper.ir

however, load–slip curve of specimen GM∗-100-2 shows a significant increase in stiffness of the joint.

Similar conclusions can be drawn by comparing different load–slip curves of tested specimens with L_f=200 mm (Fig. 8b). However, comparing the plotted diagrams of Fig. 8b with those of Fig. 8a shows that all the tested CFRP-to-masonry joints experienced larger slip values when the bond length was increased from 100 to 200 mm. Consequently, it can be concluded that increasing the FRP bond length may result in a more ductile failure in FRP–masonry joints, regardless of the bonding technique. However, due to stronger bond of FRP-to-substrate in EBROG technique, the ultimate slip of EBROG joints is rather smaller than that of conventional EBR (Fig. 8b). Furthermore, careful inspection of Fig. 8 reveals that the local debonding and load drops, emerged as constant or sudden drops in some parts of the load–slip curves, almost occurred in all the specimens, especially in WS and EB specimens. This phenomenon can be attributed to the role of mortar joints, which was comprehensively studied by Carloni and Subramaniam [4].

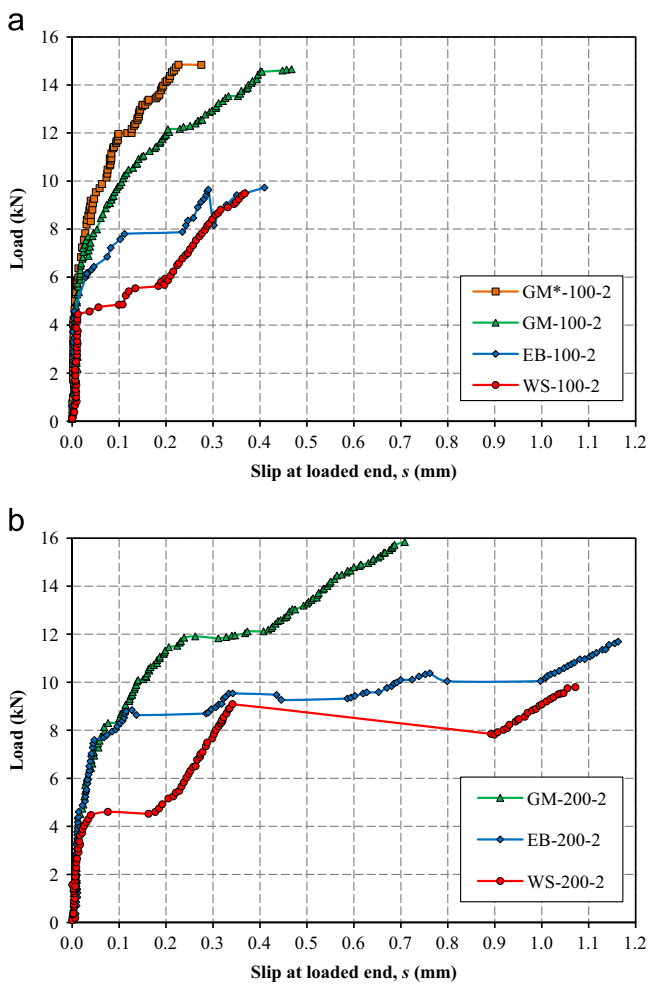

Fig. 8. Load–slip curves for series 2 specimens. (a) L_f = 100 mm. and (b) L_f = 200 mm.

4.4. Longitudinal strain profiles along the bonded length

Investigating strain distribution along bonded length of FRP reinforcement during bond tests provides valuable information to better understand the bond behavior and mechanism of stress transfer from FRP composite to masonry (concrete) substrate. Thus, evolution of strain profiles along the bonded length of CFRP sheets during loading were obtained for different bonding techniques using PIV measurements. To do so, *virtual strain gauges*, each consisted of two 256 × 256 pixel patches, having a center-to-center distance of 128 pixels (i.e. the virtual gauge length was approximately equal to 10 mm in the object space) were generated through the whole bonded length of CFRP sheets in specimens WS-100-2, EB-100-2, GM-100-2, and GM∗-100-2; and their strain profiles evolution are plotted in Figs. 9–12, respectively. Strain values are derived from the aforementioned virtual gauges for the whole length of the CFRP sheets; except for the start point of the bond length (x=0), which its corresponding strain was deduced directly from applied load values. It is due to local stress concentration at this point as previously mentioned by Hosseini and Mostofinejad [21]. As it is illustrated in Figs. 9 and 10, the obtained strain profiles in CFRP sheets of specimens WS-100-2 and EB-100-2 are almost similar during loading, which means that the stress transfer mechanism in WS and EB specimens is quite the same. On the other hand, comparing strain profile diagrams of Fig. 9 with those of Fig. 10 illustrates that in specimen WS-100-2, a sudden and brittle debonding failure occurred when the specimen reached to the ultimate load level (P/P_u=1). However, the failure in specimen EB-100-2 was a little more ductile, since strain redistribution occurred toward the free end of the CFRP sheet after reaching P/P_u=1 and before debonding failure (Fig. 10). This fact can be justified by the relatively better bond condition of CFRP-to-substrate when surface preparation was performed in EB specimens.

Similarly, evolution of strain profiles along the bonded length of CFRP sheets during loading were plotted in Figs. 11 and 12 for specimens GM-100-2 and GM∗-100-2, respectively. Comparing

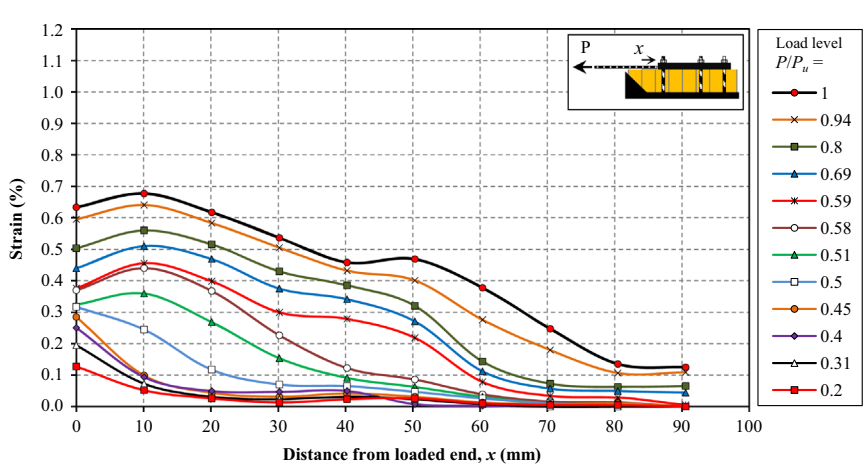

Fig. 9. Evolution of strain profile in CFRP sheet for specimen WS-100-2 (P_u=9.52 kN).

Downloaded form http://iranpaper.ir

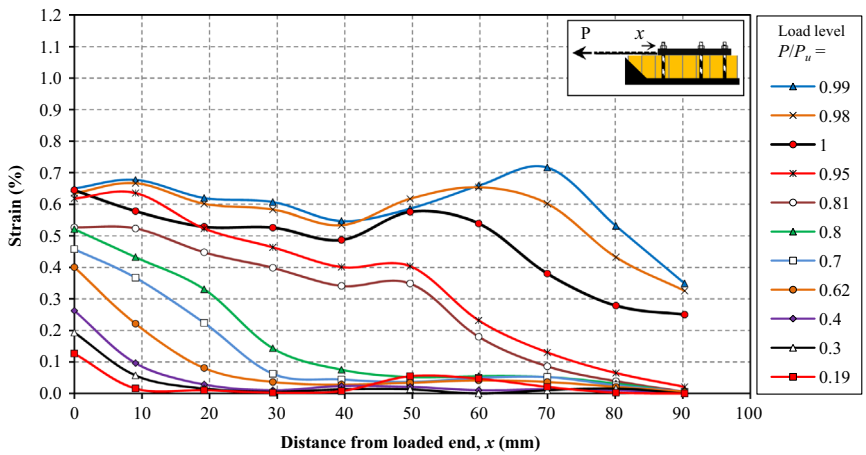

Fig. 10. Evolution of strain profile in CFRP sheet for specimen EB-100-2 (P_u=9.80 kN).

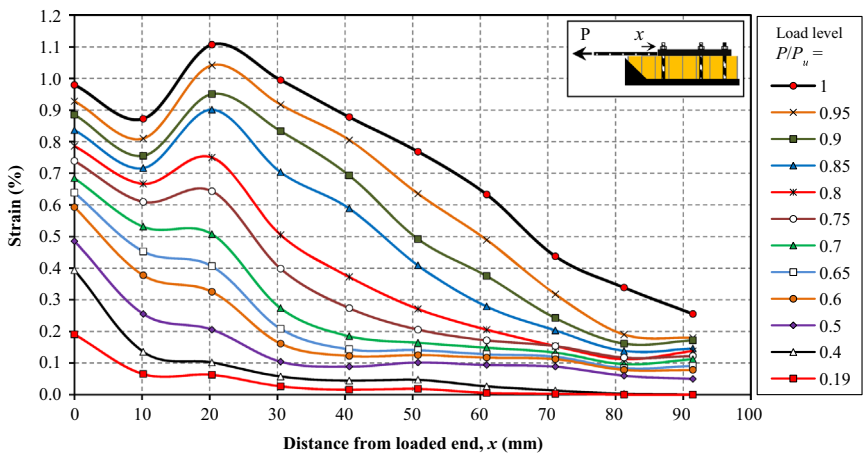

Fig. 11. Evolution of strain profile in CFRP sheet for specimen GM-100-2 (P_u=14.66 kN).

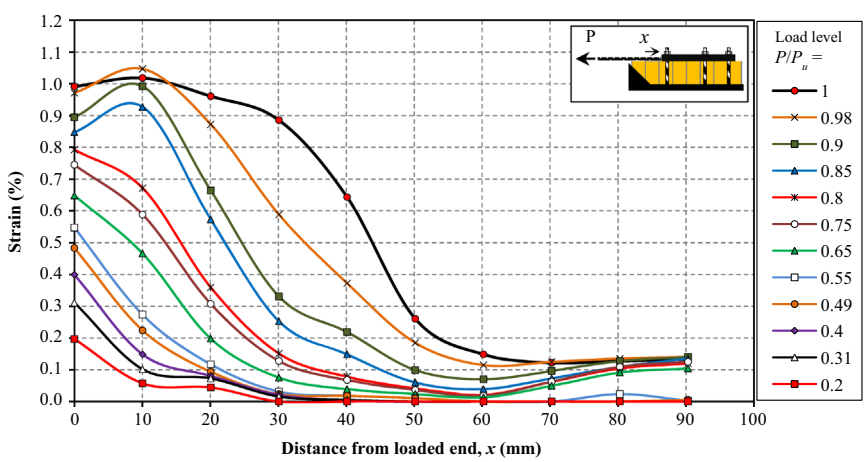

Fig. 12. Evolution of strain profile in CFRP sheet for specimen GM*-100-2 (P_u=14.89 kN).

the strain distribution along CFRP reinforcements of EBR joints (Figs. 9 and 10) with those of EBROG joints (Figs. 11 and 12) clearly shows the superiority of GM over conventional EBR; since significantly higher strain levels were obtained in CFRP sheets of GM specimens compared to those of WS and EB specimens. Furthermore, comparing strain profiles of specimen GM-100-2 plotted in Fig. 11 with those of specimen GM*-100-2 with wider grooves depicted in Fig. 12 clearly demonstrates that wider grooves better transmit interfacial shear stresses from FRP reinforcement to masonry substrate. It can be deduced from Figs. 11 and 12 that the effective bond zone of CFRP reinforcement in specimen GM*-100-2 was comparatively smaller than that of specimen GM-100-2.

Careful inspection of Figs. 11 and 12 also reveals that the peak of the strain profiles shifted few millimeters toward the free end of the FRP reinforcements by increasing the applied load; which is due to the fact that local debonding occurred through the first few

Downloaded form http://iranpaper.ir

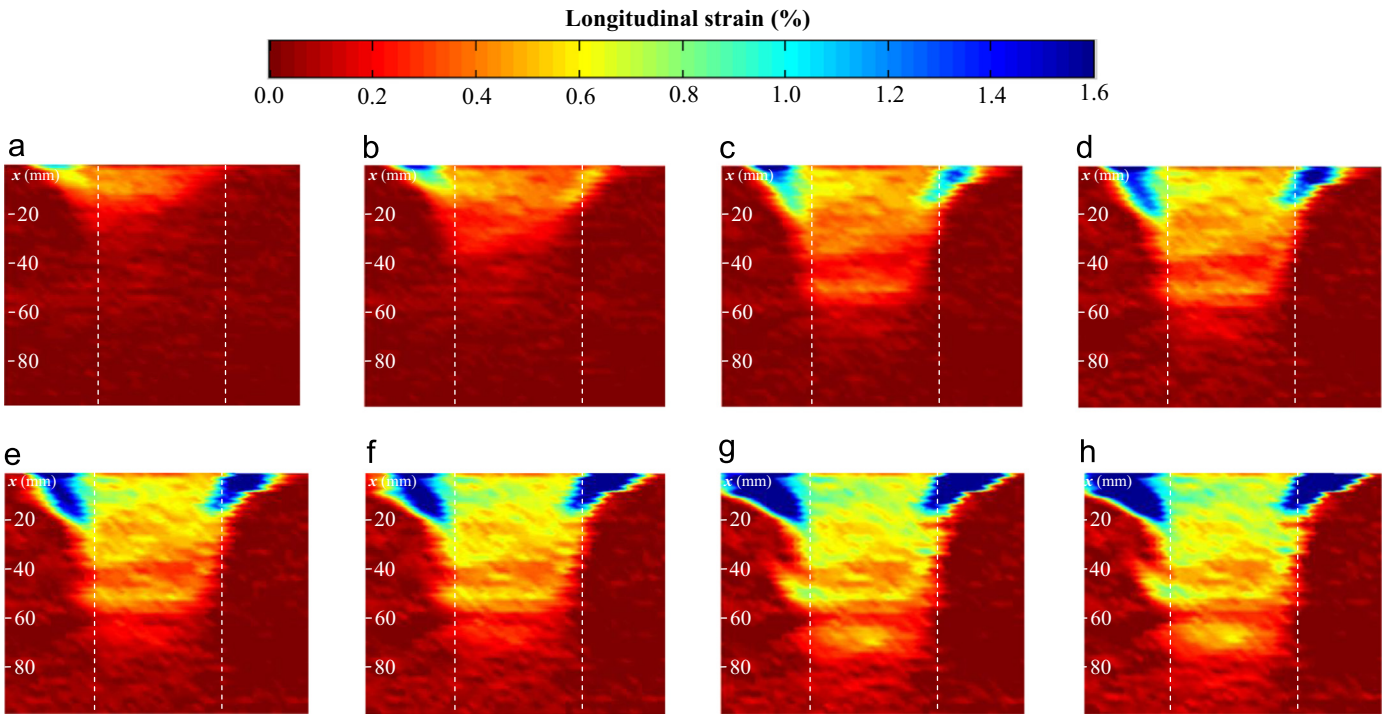

Fig. 13. Evolution of longitudinal strain field of specimen WS-100-2 during loading process (dash lines indicate 48 mm width of CFRP strip, P_u=9.52 kN). (a) 0.50 P_u, (b) 0.51 P_u, (c) 0.59 P_u, (d) 0.69 P_u, (e) 0.80 P_u, (f) 0.89 P_u, (g) 0.98 P_u and (h) P_u.

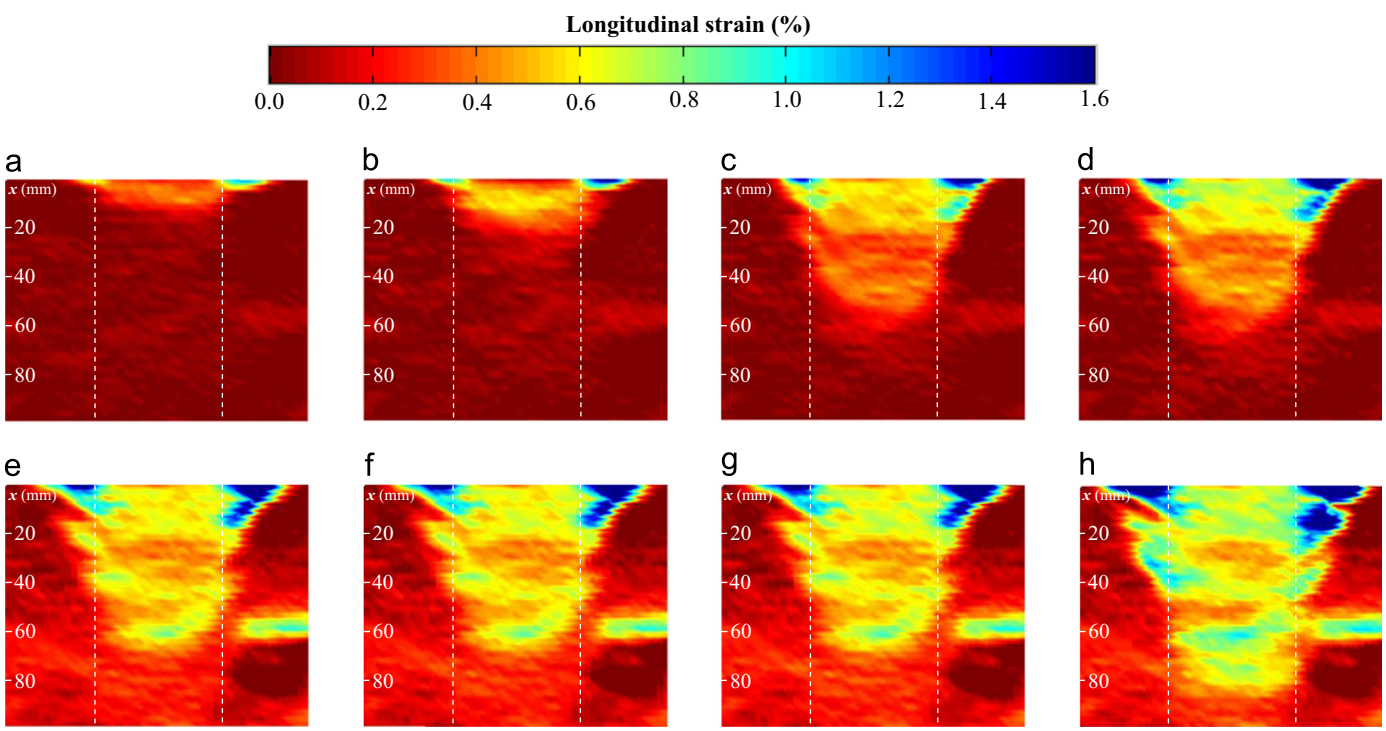

Fig. 14. Evolution of longitudinal strain field of specimen EB-100-2 during loading process (dash lines indicate 48 mm width of CFRP strip, P_u=9.80 kN). (a) 0.65 P_u, (b) 0.80 P_u, (c) 0.81 P_u, (d) 0.95 P_u, (e) P_u, (f) 0.84 P_u (post-peak), (g) 0.91 P_u (post-peak) and (h) 0.99 P_u (post-peak).

millimeters of the bond length. However, no sudden strain redistribution occurred toward the free end of the CFRP reinforcements in specimens GM-100-2 and GM∗-100-2 up to the ultimate load level. This fact again demonstrates the stronger bond of CFRP-to-masonry in EBROG technique compared to that in EBR joints.

4.5. Longitudinal strain fields

Longitudinal strain fields of tested specimens corresponding to each digital image can be also obtained utilizing full field measurements of PIV. Thus, in order to further investigate strain

Downloaded form http://iranpaper.ir

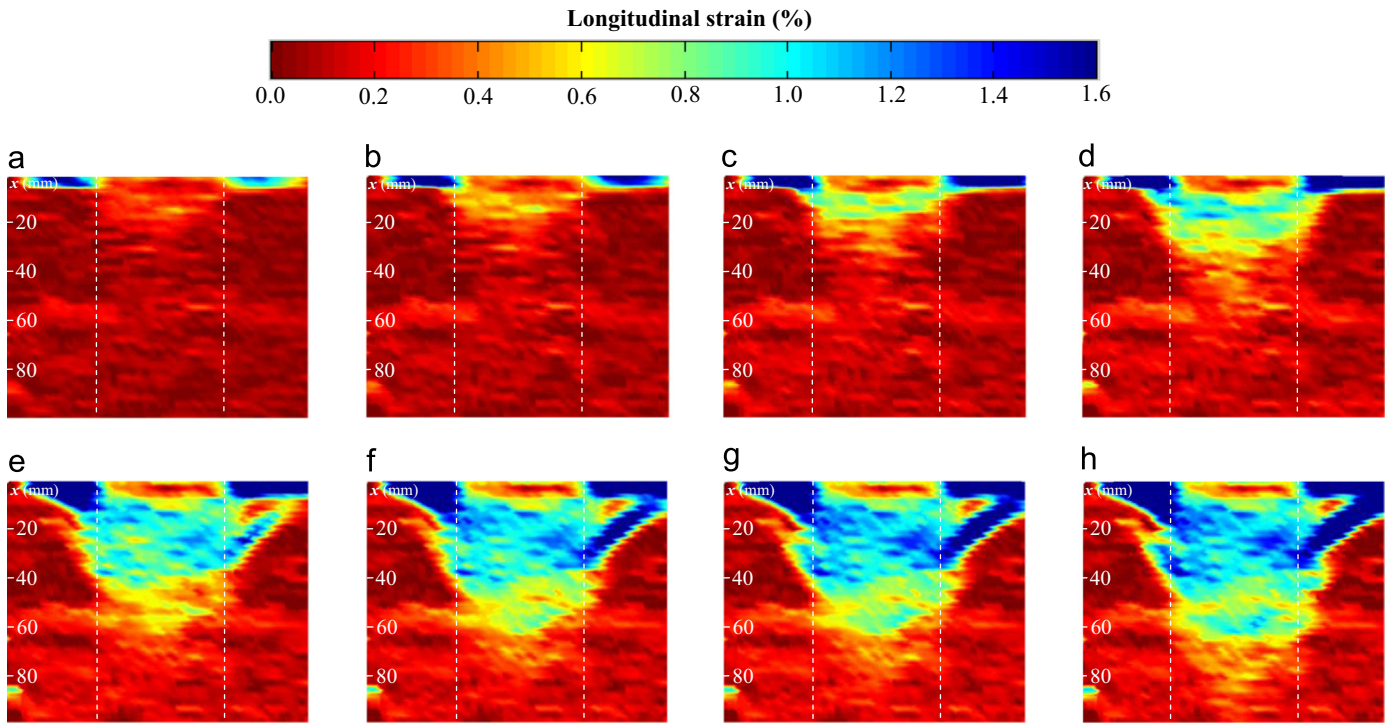

Fig. 15. Evolution of longitudinal strain field of specimen GM-100-2 during loading process (dash lines indicate 48 mm width of CFRP strip, P_u=14.66 kN). (a) 0.50 P_u, (b) 0.60 P_u, (c) 0.71 P_u, (d) 0.80 P_u, (e) 0.90 P_u, (f) 0.95 P_u, (g) 0.99 P_u and (h) P_u.

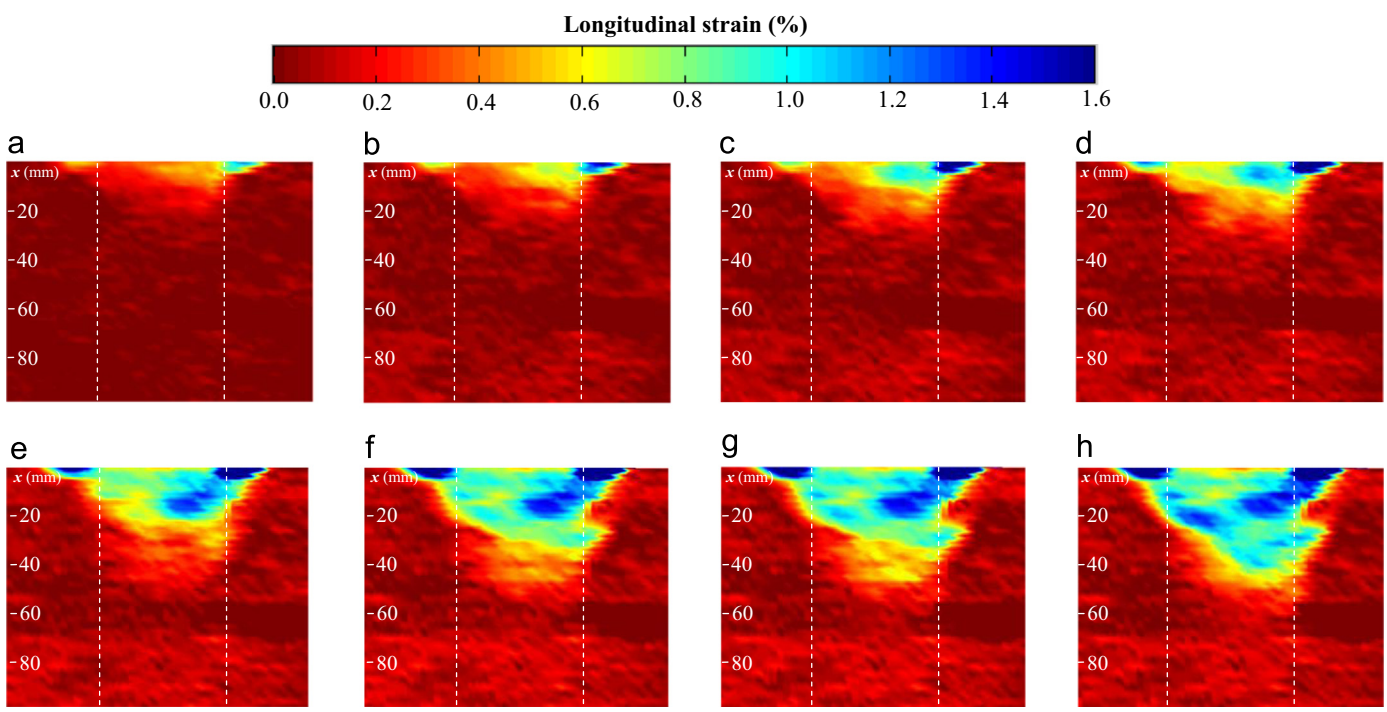

Fig. 16. Evolution of longitudinal strain field of specimen GM*-100-2 during loading process (dash lines indicate 48 mm width of CFRP strip, P_u=14.89 kN). (a) 0.55 P_u, (b) 0.61 P_u, (c) 0.71 P_u, (d) 0.80 P_u, (e) 0.90 P_u, (f) 0.98 P_u, (g) 0.99 P_u and (h) P_u.

distribution along the CFRP reinforcements as well as the local effects in the bond zone, successive digital images which were captured during the loading procedure were analyzed. An area of 125×100 mm^2 (width $\times$ length) was considered for each specimen and patches of 128×128 pixels spaced at 32 pixels center-to-center were generated. Moreover, a search area of 10×10 pixels for each pair of successive images was considered in all PIV analyses which provided sufficient area to give good tracking of the patches. Further information on the PIV procedure and strain calculations can be found in [21,22,25,32].

Longitudinal strain fields corresponding to different load levels for specimens WS-100-2 and EB-100-2 are illustrated in Figs. 13 and 14, respectively. As it is shown in Fig. 13, strain field in specimen WS-100-2 gradually distributed along the CFRP sheet up to the maximum load level (Fig. 13h). However, upon reaching P_u, debonding failure suddenly occurred; therefore, no more images could be captured

Downloaded form http://iranpaper.ir

from the field. As a consequence, probable strain redistribution in the CFRP reinforcement could not be detected due to the brittle debonding failure in WS specimens. On the other hand, evolution of longitudinal strain field in specimen EB-100-2 illustrates that a more ductile failure occurred in this specimen (Fig. 14). As it is shown in Fig. 14, strain distribution in the CFRP reinforcement of specimen EB-100-2 is almost similar to those of specimen WS-100-2 up to P_u (Fig. 14e); while after reaching P_u, a sudden load drop was observed (Fig. 14f). Afterwards, strain redistribution occurred along the CFRP reinforcement toward the free end, leading to detachment of the strip. Careful scrutiny of Fig. 14 reveals that some signs of mortar joint failure, appeared as high tensile stresses, can be detected from the provided strain fields (see strain fields of Fig. 14 between $x=50$ and 60 mm). This may be the result of poor workmanship during construction of the masonry prisms, which finally resulted in mortar joint failure in specimens EB-100-2 and GM∗-100-1 as discussed before. Furthermore, it can be concluded from the obtained strain fields in Figs. 13 and 14 that the effective bond length, L_e, of externally bonded CFRP sheets in WS and EB specimens was approximately equal to 70 mm.

Similarly, evolution of longitudinal strain fields of specimens GM-100-2 and GM∗-100-2 are illustrated in Figs. 15 and 16, respectively. Comparing the strain fields of CFRP reinforcements bonded to masonry using EBROG technique (Figs. 15 and 16) with those using conventional EBR method (Figs. 13 and 14) clearly shows that higher strain values can be reached when EBROG technique was used. Moreover, inspection of the obtained strain fields in Figs. 15 and 16 proves the fact that due to the strong bond of CFRP-to-masonry, no redistribution of strain occurred in GM specimens up to P_u. On the other hand, comparing strain fields of specimen GM∗-100-2 in Fig. 16 with those of specimen GM-100-2 in Fig. 15, demonstrates that increasing the grooves width results in considerable reduction of effective bond zone. As it is illustrated in Fig. 16h, the effective bond length of the utilized CFRP reinforcement in EBROG technique, L_e^*, was approximately equal to 50 mm in specimen GM∗-100-2 with $b_g=10$ mm; while L_e^* was approximately equal to 65 mm in specimen GM-100-2 with $b_g=5$ mm (Fig. 15h).

5. Conclusions

Bond behavior of CFRP sheets attached to masonry substrate using three different bonding techniques including externally bonding with and without surface preparation (named as EB and WS specimens, respectively), and grooving method (GM) in the form of EBROG technique (named as GM specimens) was examined through 14 single lap-shear tests. The experimental results were compared through ultimate load, failure mode, and bond efficiency factor, as well as full field deformation and strain field measurements using a non-contact image based technique, i.e. particle image velocimetry (PIV). Experimental results and PIV analyses, presented in the current study, allow the following conclusions to be drawn:

1) The dominant failure mode of WS and EB specimens was fracture in masonry through a thin layer of brick, while debonding in brick–adhesive interface is also probable in EBR joints without surface preparation due to poor quality of the bond. However, owing to the stronger bond of CFRP-to-masonry in GM specimens, the most probable failure mode was wedge-shaped splitting in brick at end of the FRP bond length. Furthermore, CFRP rupture was also observed in two of the tested GM specimens.
2) Bond strength of CFRP sheets attached to masonry substrate using EBROG technique was increased up to 60% over that of WS specimens strengthened by the conventional EBR method without surface preparation. On the other hand, utilizing a light grinding prior to bonding CFRP sheets to masonry substrate through EBR method slightly increased the ultimate capacity of the joint by 10%.
3) Increasing the FRP bond length, L_f, greater than the effective bond length, L_e, slightly increased the ultimate bond strength of the joint, which was attributed to the role of mortar joints, acting as transverse grooves. Furthermore, larger L_f provided a more ductile failure in FRP–masonry joints, regardless of the bonding technique.
4) It was observed that increasing the grooves width (b_g) from 5 to 10 mm has no significant effect on bond strength of CFRP-to-masonry joints. However, considering the failure mode of masonry EBROG joints, it is believed that deeper grooves can work more effectively in masonry strengthening.
5) Full field strain measurements obtained from PIV technique, which were presented in terms of load–slip diagrams, strain profiles, and full strain fields, demonstrated the superiority of EBROG technique over conventional EBR method; since higher strain levels were distributed through a smaller bond zone in EBROG joints. Furthermore, investigating full strain fields of the tested specimens verified that utilizing wider grooves can decrease the effective bond length of FRP in EBROG joints (L_e^*).
6) The average efficiency factor (defined as $\eta=\varepsilon_f/\varepsilon_{fu}$) of conventional EBR method was limited to 57%, while the factor increased up to an average value of 83% in EBROG joints. Thus, it can be concluded that EBROG technique can be used as a powerful alternative to conventional EBR method to more efficiently utilize the tensile capacity of CFRP composites used for external strengthening of unreinforced masonry structures.

References

[1] Willis CR, Yang Q, Seracino R, Griffith MC. Bond behaviour of FRP-to-clay brick masonry joints. Eng Struct 2009;31(11):2580–7.
[2] Kashyap J, Willis CR, Griffith MC, Ingham JM, Masia MJ. Debonding resistance of FRP-to-clay brick masonry joints. Eng Struct 2012;41(11):186–98.
[3] De Lorenzis L, Dimitri R, La Tegola A. Reduction of lateral thrust of masonry arches and vaults with FRP composites. Constr Build Mater 2007;21(7):1415–30.
[4] Carloni C, Subramaniam KV. FRP-masonry debonding: numerical and experimental study of the role of mortar joints. J Compos Constr 2012;16(5):581–9.
[5] Carloni C, Subramaniam KV. Investigation of the interface fracture during debonding between FRP and masonry. Adv Struct Eng 2009;12(5):731–43.
[6] Oliveira DV, Basilio I, Lourenço PB. Experimental bond behavior of FRP sheets glued on brick masonry. J Compos Constr 2010;15(1):23–41.
[7] Grande E, Imbimbo M, Sacco E. Bond behaviour of CFRP laminates glued on clay bricks: experimental and numerical study. Composites: Part B 2011;42(2):330–40.
[8] Faella C, Camorani G, Martinelli E, Paciello SO, Perri F. Bond behaviour of FRP strips glued on masonry: experimental investigation and empirical formulation. Constr Build Mater 2012;31:353–63.
[9] Basilio I, Fedele R, Lourenço PB, Milani G. Assessment of curved FRP-reinforced masonry prisms: experiments and modeling. Constr Build Mater 2014;51:492–505.
[10] Petersen RB, Masia MJ, Seracino R. Bond behavior of near-surface mounted FRP strips bonded to modern clay brick masonry prisms: influence of strip orientation and compression perpendicular to the strip. J Compos Constr 2009;13(3):169–78.
[11] Dizhur D, Griffith M, Ingham J. Out-of-plane strengthening of unreinforced masonry walls using near surface mounted fibre reinforced polymer strips. Eng Struct 2014;59:330–43.
[12] Aiello MA, Sciolti SM. Bond analysis of masonry structures strengthened with CFRP sheets. Constr Build Mater 2006;20(1):90–100.
[13] Camli US, Binici B. Strength of carbon fiber reinforced polymers bonded to concrete and masonry. Constr Build Mater 2007;21(7):1431–46.
[14] Caggegi C, Penesse V, Fagona M, Cuomo M, Chevalier L. Experimental global analysis of the efficiency of carbon fiber anchors applied over CFRP strengthened bricks. Constr Build Mater 2014;53:203–12.
[15] ACI committee 440. Guide for the design and construction of externally bonded FRP systems for strengthening concrete structures (ACI 440.2R-08). Farmington Hills, MI: American Concrete Institute; 2008.
[16] Kalfat R, Al-Mahaidi R, Smith ST. Anchorage devices used to improve the performance of reinforced concrete beams retrofitted with FRP composites: state-of-the-art review. J Compos Constr 2011;17(1):14–33.

Downloaded form http://iranpaper.ir

[17] Mostofinejad D, Mahmoudabadi E. Grooving as alternative method of surface preparation to postpone debonding of FRP laminates in concrete beams. J Compos Constr 2010;14(6):804–11.
[18] Mostofinejad D, Shameli SM, Hosseini A. Experimental study on the effectiveness of EBROG method for flexural strengthening of RC beams. In: Proceedings of sixth international conference on FRP Composites in Civil Engineering (CICE 2012), Rome, Italy; 2012.
[19] Mostofinejad D, Shameli SM. Externally bonded reinforcement in grooves (EBRIG) technique to postpone debonding of FRP sheets in strengthened concrete beams. Constr Build Mater 2013;38:751–8.
[20] Mostofinejad D, Shameli SM, Hosseini A. EBROG and EBRIG methods for strengthening of RC beams by FRP sheets. Eur J Environ Civ Eng 2014;18 (6):652–68.
[21] Hosseini A, Mostofinejad D. Experimental investigation into bond behavior of CFRP sheets attached to concrete using EBR and EBROG techniques. Composites: Part B 2013;51:130–9.
[22] Hosseini A, Mostofinejad D. Effect of groove characteristics on CFRP-to-concrete bond behavior of EBROG joints: experimental study using particle image velocimetry (PIV). Constr Build Mater 2013;49:364–73.
[23] ASTM C67-05. Standard test methods for sampling and testing brick and structural clay tile; 2005.
[24] ASTM C109/C109M-05. Standard test method for compressive strength of hydraulic cement mortars (Using 2-in. or [50-mm] cube specimens); 2005.
[25] Hosseini A, Mostofinejad D. Effective bond length of FRP-to-concrete adhesively-bonded joints: experimental evaluation of existing models. Int J Adhes Adhes 2014;48:150–8.
[26] Mazzotti C, Savoia M, Ferracuti B. An experimental study on delamination of FRP plates bonded to concrete. Constr Build Mater 2008;22(7):1409–21.
[27] Ali-Ahmad M, Subramaniam K, Ghosn M. Experimental investigation and fracture analysis of debonding between concrete and FRP sheets. J Eng Mech 2006;132(9):914–23.
[28] Carloni C, Subramaniam KV. Direct determination of cohesive stress transfer during debonding of FRP from concrete. Compos Struct 2010;93(1):184–92.
[29] Adrian RJ. Particle imaging techniques for experimental fluid mechanics. Annu Rev Fluid Mech 1991;23:261–304.
[30] White DJ, Take WA, Bolton MD. Soil deformation measurement using Particle Image Velocimetry (PIV) and photogrammetry. Geotechnique 2003;53 (7):619–31.
[31] White DJ, Take WA. GeoPIV: Particle Image Velocimetry (PIV) software for use in geotechnical testing. Technical Report, D-SOILS-TR322. Cambridge University Engineering Department; 2002.
[32] Hosseini A, Mostofinejad D, Hajialilue-Bonab M. Displacement and strain field measurement in steel and RC beams using particle image velocimetry. J Eng Mech 2014;140:11.
[33] Carloni C, Subramaniam KV. Investigation of sub-critical fatigue crack growth in FRP/concrete cohesive interface using digital image analysis. Composites: Part B 2013;51:35–43.
[34] Chen JF, Teng JG. Anchorage strength models for FRP and steel plates bonded to concrete. J Struct Eng 2001;127(7):784–91.